RESEARCH ARTICLE

[11C]Harmine Binding to Brain Monoamine Oxidase A: Test-Retest Properties and Noninvasive Quantification

Francesca Zanderigo [1,2] Alexandra E. D'Agostino,[3] Nandita Joshi,[4] Martin Schain,[1] Dileep Kumar,[2] Ramin V. Parsey,[3] Christine DeLorenzo,[3] J. John Mann[1,2,5]

[1]Department of Psychiatry, Columbia University, 1051 Riverside Drive, New York, NY, 10032, USA
[2]Molecular Imaging and Neuropathology Division, New York State Psychiatric Institute, 1051 Riverside Drive, New York, NY, 10032, USA
[3]Now at Department of Psychiatry, Stony Brook University, 101 Nicolls Road, Health Sciences Center, Level 10, Stony Brook, NY, 11794, USA
[4]Department of Electrical and Computer Engineering, Stony Brook University, Stony Brook, NY, 11794, USA
[5]Department of Radiology, Columbia University, 622 W 168th Street, New York, NY, 10032, USA

Abstract

Purpose: Inhibition of the isoform A of monoamine oxidase (MAO-A), a mitochondrial enzyme catalyzing deamination of monoamine neurotransmitters, is useful in treatment of depression and anxiety disorders. [11C]harmine, a MAO-A PET radioligand, has been used to study mood disorders and antidepressant treatment. However, [11C]harmine binding test-retest characteristics have to date only been partially investigated. Furthermore, since MAO-A is ubiquitously expressed, no reference region is available, thus requiring arterial blood sampling during PET scanning. Here, we investigate [11C]harmine binding measurements test-retest properties; assess effects of using a minimally invasive input function estimation on binding quantification and repeatability; and explore binding potentials estimation using a reference region-free approach.

Procedures: Quantification of [11C]harmine distribution volume (V_T) *via* kinetic models and graphical analyses was compared based on absolute test-retest percent difference (TRPD), intraclass correlation coefficient (ICC), and identifiability. The optimal procedure was also used with a simultaneously estimated input function in place of the measured curve. Lastly, an approach for binding potentials quantification in absence of a reference region was evaluated.

Results: [11C]harmine V_T estimates quantified using arterial blood and kinetic modeling showed average absolute TRPD values of 7.7 to 15.6 %, and ICC values between 0.56 and 0.86, across brain regions. Using simultaneous estimation (SIME) of input function resulted in V_T estimates close to those obtained using arterial input function ($r = 0.951$, slope = 1.073, intercept = – 1.037), with numerically but not statistically higher test-retest difference (range 16.6 to 22.0 %), but with overall poor ICC values, between 0.30 and 0.57.

Conclusions: Prospective studies using [11C]harmine are possible given its test-retest repeatability when binding is quantified using arterial blood. Results with SIME of input function

---

Correspondence to: Francesca Zanderigo; *e-mail:* Francesca.Zanderigo@nyspi.columbia.edu

show potential for simplifying data acquisition by replacing arterial catheterization with one arterial blood sample at 20 min post-injection. Estimation of [^{11}C]harmine binding potentials remains a challenge that warrants further investigation.

Introduction

Monoamine oxidase (MAO), a mitochondrial enzyme involved in the oxidative deamination of monoamine neurotransmitters, plays a central role in regulating neurotransmitter levels such as dopamine, norepinephrine and serotonin [1–3]. The isoenzyme MAO-A preferentially acts on serotonin and noradrenaline, and in human brain, it is predominantly localized in norepinephrine, serotoninergic, and dopaminergic neurons, astrocytes and glia cells [4]. Inhibition of MAO-A has been shown to be useful in treatment of major depression and anxiety disorder [5], in agreement with the monoamine theory of depression [6].

Among the several radiotracers developed for use with Positron Emission Tomography (PET) for quantification of MAO-A levels *in vivo* [7–13], [^{11}C]harmine has shown promising characteristics. [^{11}C]harmine binds selectively and reversibly to the isoenzyme MAO-A ($K_i = 5$ nmol/l [13, 14]) and displays favorable *in vivo* pharmacokinetic properties [12, 15].

In the past two decades, [^{11}C]harmine has been used for quantification of MAO-A binding in several investigations, including during a major depressive episode [6, 16], before and after antidepressant treatment with selective serotonin reuptake inhibitors [17], moclobemide, and St. John's wort [18], in the early postpartum period [19], in relation to changes in MAO-A substrate [20], in antisocial personality disorder [21], and borderline personality disorder [22].

Despite this body of work, test-retest characteristics of [^{11}C]harmine binding to brain MAO-A have been only partially investigated to-date and quantification methods that aim at reducing the need for arterial sampling have not been explored. Ginovart et al. [23] investigated [^{11}C]harmine quantification in five subjects who were scanned twice, after 10 days treatment with placebo and after 10 days treatment with moclobemide, with a between-conditions period of at least 8 weeks. Quantification with one-tissue compartment (1TC) [24] and variants of the two-tissue compartment (2TC) model was compared to that obtained from Logan graphical analysis (Logan) [25], but no test-retest characteristics were reported. Sacher et al. [18] included two repeated scans in a group of 10 healthy controls, but the time period between measurements was 6 ± 12 weeks, and the test-retest analysis confined to total distribution volume (V_T) [26] obtained using the 2TC model. V_T represents the sum of radiotracer specific binding to the target and non-displaceable binding, and its estimation requires measuring the arterial input function during the course of the PET scan. Arterial sampling is invasive, prone to measurement errors, increases the risk for adverse events, and may be uncomfortable for the subject. However, since MAO-A is ubiquitously expressed [23, 27, 28], there is no valid reference brain region, and therefore acquisition of the arterial input function is currently the only option for full quantification of [^{11}C]harmine.

The aims of our study were to (1) assess test-retest properties of [^{11}C]harmine binding measurements using data from healthy volunteers imaged twice, on the same day; (2) quantify effects of using a less-invasive estimation of input function instead of arterial blood sampling on [^{11}C]harmine binding quantification and repeatability; and (3) investigate whether it is possible to estimate [^{11}C]harmine binding potentials (BP$_P$, BP$_F$, and BP$_{ND}$ [26]) using a reference region-free quantification approach [29].

Materials and Methods

Sample

Five healthy male volunteers, aged 18–65 years, gave informed written consent to participate in a protocol approved by the New York State Psychiatric Institute Institutional Review Boards. Eligibility assessment included medical and psychiatric history, physical examination, blood tests, urinalysis, urine toxicology, and electrocardiogram. The Structured Clinical Interview for DSM-IV Axis I Disorders (non-patient version-SCID NP) [30] was used to rule out psychiatric disorders. Inclusion criteria included (1) age 18–65 years; (2) absence of Axis I disorder; (3) absence of lifetime history of alcohol or substance use disorders; (4) absence of lifetime IV drug use or 3,4-methylenedioxy-methamphetamine use more than twice; (5) absence of significant medical conditions; and (6) capacity to provide informed consent. All participants were off anti-coagulant/anti-platelet treatment, with exception of aspirin, for 10 days prior to PET imaging. Exclusion criteria included (1) pregnancy, currently lactating, planning to conceive during the study participation or abortion in the past 2 months; (2) dementia (clinical and neurocognitive criteria, Folstein Mini Mental State Examination > 25); (3) a neurological disease or lifetime history of head injury involving loss of consciousness or motor deficits; (4) claustrophobia; (5) recent (< 7 days) consumption of Ayahuasca Tea or other South American non-standard decoction; (6) presence of metallic devices, implants, and other contraindications to scanning; (7) current, past, or anticipated exposure to radiation (*e.g.*, in the workplace,

participation in nuclear medicine research protocols, exposure to radioactive substances or radiation including more than one diagnostic x-ray in the year before PET imaging); (8) use of tobacco products in the previous 3 months; (9) presence and/or history of clinically significant major neurological or psychiatric disorders in first-degree relatives; and (10) > two first-degree relatives with history of substance dependence.

Magnetic Resonance Imaging Acquisition

All subjects underwent a three-dimensional fast spoiled gradient recalled acquisition (FSPGR) T1-weighted axial Magnetic Resonance (MR) scan, acquired using a 3 T Signa Advantage system (General Electric Medical Systems, Milwaukee, Wisconsin) within a few weeks of the PET scan, for definition of anatomic regions of interest (ROIs). The sequence parameters were TR ~ 7 s, TE 2.3–3 ms, flip angle 9 °, slice thickness 1.0 mm, acquisition matrix 256 × 256, 1.02 × 1.02 × 1.00 mm^3 voxels. Detailed quality control using visual inspection was carried out to rule out substantial motion artifacts and gross neuropathology.

MRI Image Processing

Raw MR images were cropped to remove non-brain tissue using Atropos (http://www.picsl.upenn.edu/ANTs) [31] and segmented using statistical parametric mapping software (http://www.fil.ion.ucl.ac.uk/spm/software/). An automated algorithm was used to identify ROIs, as previously described [32]. Anatomical ROIs were traced on individuals' T1-weighted MRs *via* an automatic approach that uses either an in-house atlas created from hand-drawn ROIs of 18 subjects or from the LPBA40/SPM5 probabilistic brain atlas, based on 40 labeled brains [33]. Eleven ROIs were considered based on previous studies with this radiotracer [6, 16–18, 23] for evaluation of test-retest repeatability: thalamus, midbrain, anterior cingulate, hippocampus, ventral striatum, medial prefrontal cortex (PFC), temporal lobe, dorsal putamen, dorsolateral and orbital PFC, and cerebellar gray matter. In the application of simultaneous estimation of input function (described below), ROIs for the dorsal caudate and entorhinal cortex were also included. Time activity curves (TACs) were defined as the average radioactivity measured within each ROI over the time course of the PET acquisition.

PET Radiochemistry and Input Function Measurement

All participants were scanned with [^{11}C]harmine twice in the same day (morning and afternoon). [^{11}C]harmine was synthesized as described in [15]. For each scan, arterial and venous catheters were placed for blood sampling and radioligand injection, respectively. Arterial blood samples were collected during the PET acquisitions for measurement of radiotracer parent fraction and metabolite-corrected

plasma input functions. An automated blood sampling system collected arterial samples in heparinized tubes every 10 s for the first 2 min and every 20 s between 2 and 4 min. Thereafter, 11 samples were collected manually at 6, 8, 12, 16, 20, 30, 40, 50, 75, 95, and 120 min post-injection in sodium heparin collection tubes (BD Vacutainer). Each blood sample was centrifuged in a Hamilton Bell Vanguard V6500 (10 min at 1800 g), and the plasma supernatant was collected in 200 ml aliquots. These aliquots were positioned in a well counter (Wallach 1480 Wizard 3 M Automatic Gamma Counter) to measure plasma radiotracer concentration. The parent fraction was measured in six of the collected samples (at 2, 6, 20, 50, 75, and 95 min) using high-performance liquid chromatography (HPLC) equipped with a radioactivity detector. The metabolite and parent [^{11}C]harmine fractions were collected based on a Bioscan gamma detector and assayed on a Packard Instruments Gamma Counter (Model E5005). All acquired data were subjected to correction for background radioactivity and physical decay to calculate the [^{11}C]harmine percentage in plasma at different time points. These resulting parent fraction curves were then fitted with a Hill function [34] to estimate the values at intermediate time points. The Hill function was selected as it provided better fits than other considered functions, such as one- and two-decreasing exponentials and power function damping [35]. The metabolite-corrected arterial input function was calculated as the product of the fitted parent fraction curve and total plasma counts. The input function was fitted using a linear interpolation before the peak and the sum of three-decreasing exponentials after the peak.

PET Image Acquisition and Analysis

PET images were acquired from an ECAT EXACT HR+ scanner (Siemens/CTI, Knoxville, Tennessee) as previously described [36]. To prevent head movement during scan, individual polyurethane molds (Soule Medical, Tampa, FL, USA) were poured around each subject's head. A 15-min transmission scan was obtained prior to radiotracer administration, followed by an intravenous bolus injection of [^{11}C]harmine (max injected dose: 20 mCi; max injected mass: 9 microgram) performed over 30 s using an automated pump (Graseby 3400 Syringe Pump, Graseby 3000, Watford, UK; bolus infusion rate: 1200 ml/h). Emission data were collected in 3D mode for 120 min and binned into 21 time frames of increasing duration (3 × 20 s, 3 × 1 min, 3 × 2 min, 2 × 5 min, 10 × 10 min). PET images were reconstructed using filtered back projection, into a 128 × 128 image matrix size (pixel size 1.72 × 1.72 mm), with a Shepp filter of 2.5 mm full width at half maximum (FWHM), a Z-filter of 2 mm FWHM, and a zoom factor of 4. Scattered events were corrected for using monte-carlo based simulation approach [37]. The final resolution of the images was 5.1 mm FWHM at the center of the field of view [38]. To correct for residual subject motion during scanning, PET

frames were registered to the eighth frame using the FMRIB linear image registration tool (FLIRT) version 5.0 (FMRIB Image Analysis Group, Oxford, UK). Each participant's mean PET image was co-registered to the corresponding MR using FLIRT with a mutual information cost function, six degrees of freedom, and trilinear interpolation, optimized as previously described [32].

PET Outcome Measure Estimation

Four approaches were considered for TACs quantification: 1TC and 2TC model [24, 39], Logan [25], and likelihood estimation in graphical analysis (LEGA) [40]. All approaches involved a metabolite-corrected arterial input function. The same weighting scheme (weights equal to the square root of each frame duration) was applied in all approaches. TACs were corrected for vascular contribution using a fixed fractional blood volume of 5 % before applying each of the quantification approach. The optimal t^* for Logan and LEGA varies across subjects and regions from a minimum of $t^* = 9$ min to a maximum of $t^* = 45$ min (plots are reported in the Supplementary Material). t^* was therefore set to 45 min post-injection in order to allow all considered regions and scans to reach the "linear phase" in the Logan plot. The radiotracer V_T [26] was considered the primary outcome measure. Analyses were performed using Matlab 2012b (www.mathworks.com/).

Metrics for Comparison of Quantification Approaches

Goodness of Fit

For the two compartment models, goodness of fit was evaluated using the weighted residual sum of squares (WRSS) and the Akaike Information Criterion (AIC) [41].

Test-Retest Percent Difference (TRPD)

Test-retest repeatability was calculated as the absolute difference between the test and retest outcome measure values, divided by their average.

Intraclass Correlation Coefficient

The measure of within-subject variability relative to between-subject variability, the intraclass correlation coefficient (ICC), was computed [42].

Identifiability

In each scan and ROI, we computed 100 bootstrap samples of the TACs data as described in [43], and estimated V_T in each of these samples using the four quantification approaches, in order to compare their stability in modeling the TACs. Similar to

previous studies [44], the variability of these V_T estimates was assessed using the median absolute deviation (MAD) criterion: $MAD = median[|Z_j - median(Z_1, Z_2, \ldots, Z_{100})|, j = 1, 2, \ldots, 100]$. This approach for determining identifiability does not rely on assumptions on noise distribution and is an alternative to methods in nonlinear regression that are based on asymptotic formulas of the standard error.

Time Stability

Considerations of subject comfort as well as minimizing experimental costs motivate using acquisition times as short as possible. All acquisitions analyzed here included 120 min of scanning. To assess performance of each quantification method for shorter scan durations, each approach was applied to data with later frames deleted, carried out for total scan times of 110, 100, 90, 80, and 70 min. For each ROI, the ratio between V_T obtained with reduced scan time and that for the full scan was calculated. A quantification procedure for a given ROI was considered stable at a given scanning duration if the mean of these ratios across scans was between 0.95 and 1.05, and if a plateau was reached [44]. TRPD and ICC values were calculated for V_T estimates obtained with shortened scanning durations.

Simultaneous Estimation of Input Function

To investigate whether unbiased estimates of V_T could be obtained without arterial catheterization, quantification of the [^{11}C]harmine data was also performed using a less-invasive quantification approach proposed by our group, the simultaneous estimation (SIME) of input function [45], which only requires one blood sample for identifiability of the metabolite-corrected input function. Samples from four different time points (at 6, 20, 50, and 95 min post-injection) were considered. In order to simultaneously consider kinetics as distinct as possible within SIME [45], we used TACs data from 7 ROIs: cerebellar gray matter, dorsal caudate, dorsal putamen, entorhinal cortex, hippocampus, temporal lobe, and thalamus. The metabolite-corrected input function obtained *via* SIME was then used with 1TC and 2TC models, Logan and LEGA to estimate V_T. In each region and scan, percent difference from blood-based V_T estimates was calculated as the absolute difference between blood-based V_T and SIME-derived V_T values, divided by blood-based V_T, multiplied by 100. Test-retest characteristics of noninvasive estimates were compared to those obtained *via* blood-based quantification.

Estimation of Non-displaceable Distribution Volume and Specific Binding Potentials in Absence of a Reference Region

The absence of a reference region precludes indirect determination of [^{11}C]harmine non-displaceable distribution

volume (V_{ND}) and thus of binding potentials BP_P, BP_F, and BP_{ND} [26]. We quantified V_{ND} and BP_P directly from the estimated 2TC kinetic rates as $V_{ND} = \frac{K_1}{k_2}$ and $BP_P = \frac{K_1 k_3}{k_2 k_4}$, respectively, and calculated their test-retest properties. We also applied our parametric approach to quantification of V_{ND} and BP_P in absence of a reference region [29].

Results

Sample and Radiochemistry

The study sample consisted of five male healthy controls, aged 20–45 years at time of imaging (mean 36 years, SD 11). Demographics and experimental details are described in Table 1. Specific radioactivities of injected dose ranged between 0.43 and 1.88 mCi/nmol (mean 1.41 mCi/nmol; SD 0.46 mCi/nmol). Injected masses of unlabeled harmine ranged between 0.98 and 8.91 μg (mean 5.18 μg; SD 2.30 μg). A two-tailed paired t-test showed no statistically significant differences in dose, specific radioactivity, and mass injected at test and retest scans.

Parent Fraction Curves

[^{11}C]Harmine parent fraction values [23], average $\pm$ SD across the 10 scans, were (in %) 98.04 ± 1.39, 69.85 ± 9.74, 34.10 ± 7.45, 16.32 ± 4.29, 12.91 ± 3.06, and 10.50 ± 4.08 at 2, 6, 20, 50, 75, and 95 min post-injection, respectively. A Hill function [34] provided good fit of all parent fraction curves in the dataset (Fig. 1).

Total Plasma Radioactivity and Metabolite-Corrected Input Function Curves

Measured plasma total radioactivity curves were consistent between each test and retest scan (Fig. 2). The adopted input function model (i.e., linear rise before the peak, tri-exponential decay after) provided good fit of all metabolite-corrected input function data.

Time Activity Curves Goodness of Fit and Total Distribution Volume Estimates

The 1TC and 2TC models provided very similar fits. Figure 3 reports measured and fitted TACs in the 11 reported ROIs in a representative subject.

V_T estimates obtained with 1TC and 2TC models were similar and comparable to those obtained from graphical approaches (Fig. 4a): paired two-tail t-test, region by region, revealed no statistically significant differences between any of the quantification methods (p values ranged between 0.44 and 0.99). Regression analyses with V_T estimates from 1TC (across ROIs and subjects) as independent variable, and V_T estimates from the other quantification methods as dependent variable, yield the following: correlation $r = 1.000$, slope $= 1.001$, intercept $= 0.018$ (1TC vs. 2TC); correlation $r = 0.989$, slope $= 0.922$, intercept $= 0.554$ (1TC vs. Logan); correlation $r = 0.991$, slope $= 0.962$, intercept $= 0.456$ (1TC vs. LEGA).

Test-Retest Percent Difference and Intraclass Correlation Coefficient

TRPD values obtained for V_T estimates quantified using 1TC and 2TC are, on average, between 7.7 and 15.6 % across ROIs. These values were somewhat numerically lower than those obtained for Logan and LEGA (range 9.6 to 16.3 %) (Fig. 4b). There is variability of TRPD values across subjects (Fig. 4c); subject 4 shows the highest TRPD values, likely due to a failure in sampling the radioactivity curve peak in blood in the retest scan (Fig. 2). In this limited sample size, no significant difference in test-retest variability between the methods was observed (paired two-tail t-test; p values ranged between 0.51 and 0.99).

Excellent (> 0.75) ICC values were obtained for V_T estimated using all 4 approaches in medial PFC, dorsal putamen, dorsolateral and orbital PFC, and gray matter cerebellum (between 0.75 and 0.86), while acceptable values (> 0.5) are obtained in the remaining regions (between 0.55 and 0.75) (Fig. 4d).

Table 1. Demographics and injected radiochemical variables of the study samples. *T* test, *RT* retest, *M* male, *SD* standard deviation

| Participant no.	Age	Gender	Injected dose (mCi)		Injected mass (μg)		Specific radioactivity (mCi/nmol)	
			T	RT	T	RT	T	RT
1	29	M	11.34	17.60	8.58	4.80	0.43	1.29
2	43	M	3.03	15.89	0.98	4.32	1.52	1.70
3	20	M	16.19	17.34	4.70	5.30	1.82	1.50
4	45	M	17.52	17.11	3.82	6.07	1.74	1.43
5	45	M	15.95	16.12	4.28	8.91	1.88	0.83
Average	36.4		12.81	16.81	4.47	5.88	1.48	1.35
SD	11.3		5.94	0.76	2.72	1.81	0.60	0.32
Min	20		3.03	15.89	0.98	4.32	0.43	0.83
Max	45		17.52	17.60	8.58	8.91	1.88	1.70
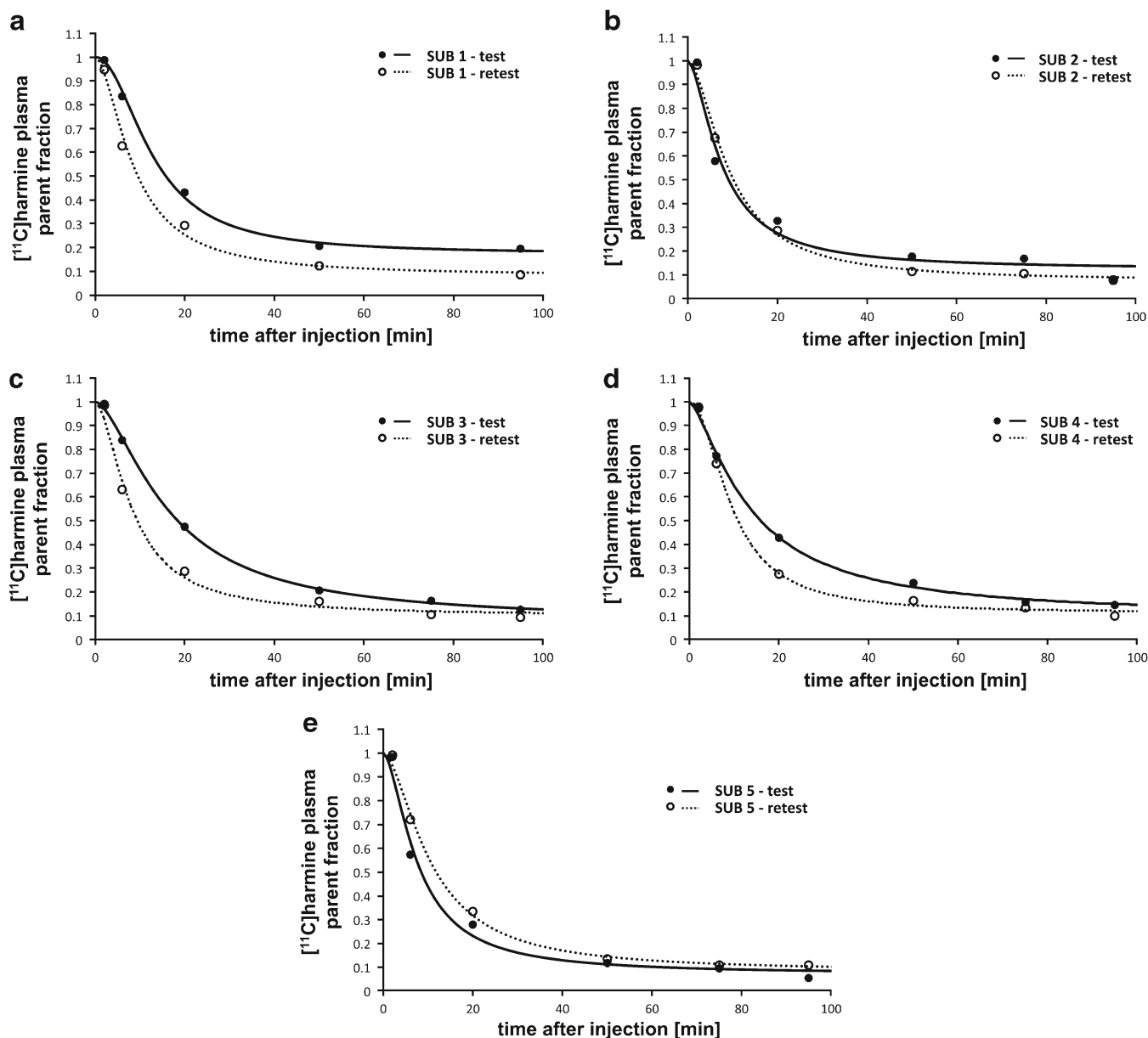
Fig. 1 a–e Parent fractions of [^{11}C]harmine determined in test (●) and retest (○) scan for five subjects. A Hill function [34] provided good fit of all parent fraction curves in the dataset.

Identifiability and Time Stability Analysis

Identifiability was comparable between 1TC and 2TC model (range of MAD values 0.08 to 0.24 across ROIs), with the latter providing slightly lower MAD values (*i.e.*, better identifiability) in five of the considered ROIs. While identifiability of Logan was the poorest among considered methods (range of MAD values across ROIs 0.21 to 0.38), LEGA resulted in MAD values that were comparable or lower (*i.e.*, comparable or superior identifiability) to those obtained with 1TC and 2TC model across considered ROIs (range of MAD values 0.08 to 0.23). Note that bootstrapping of the residuals was carried out using a different number of data points for the 1TC and 2TC model (21 data points) *vs.* the two graphical approaches, for which only eight data

points in the linear phase are considered. As bootstrapping for graphical approaches uses a lower number of residuals than it does for the kinetic models, the results may be naturally more variable [43].

Time stability analysis revealed that V_T estimates increase as the time of scanning shortens for all four considered quantification methods and all regions, without reaching a plateau (Fig. 5). This increase is more pronounced with the graphical approaches, whose estimation of V_T depends more heavily than that from compartment models on the number of data points included in the regression. With shorter scan duration, fewer data points will be used for a given t*. Furthermore, while Ginovart et al. report that relatively stable tissue-to-plasma ratios over time were observed in five subjects [23], these ratios slowly decrease over time in
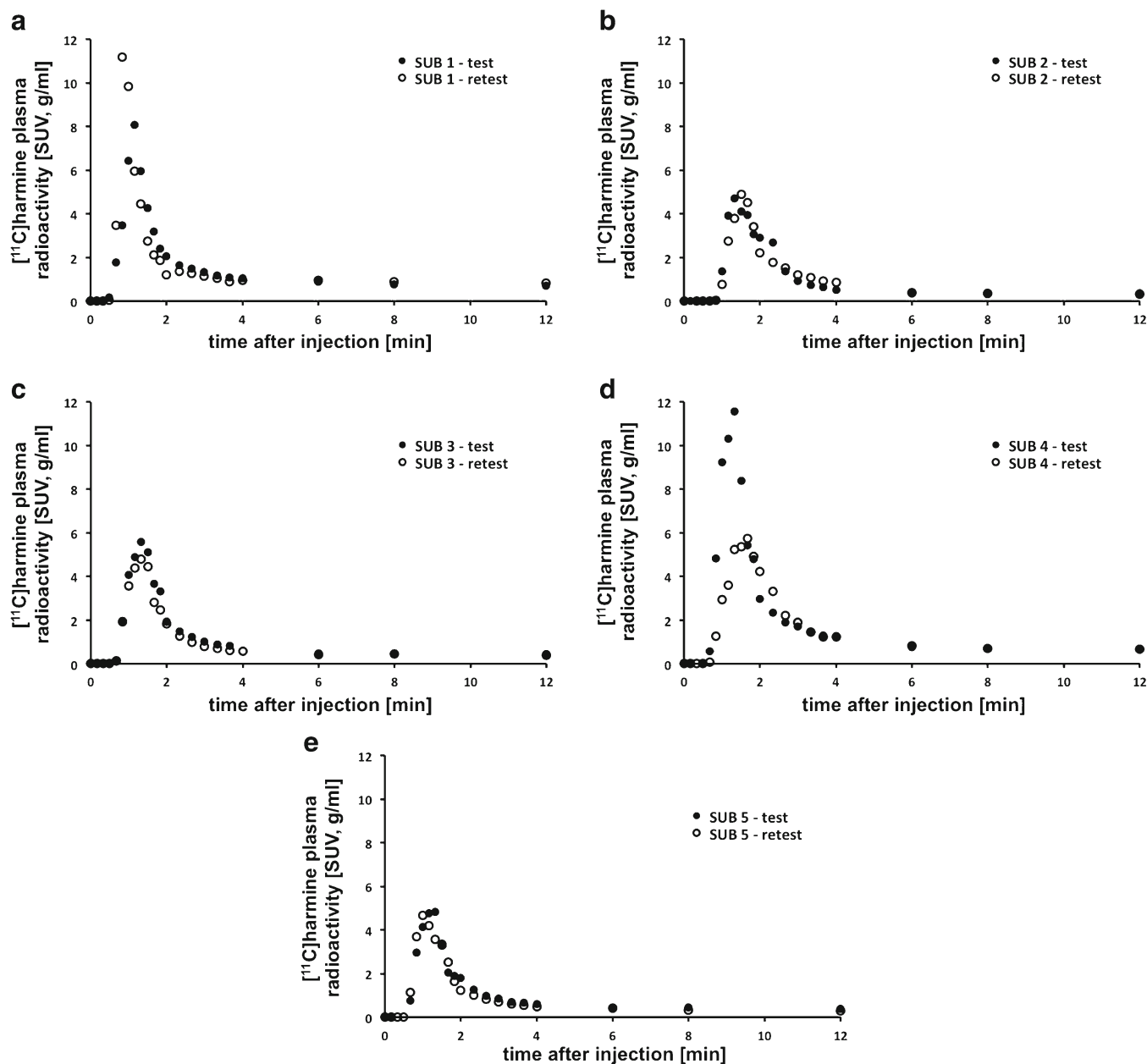
Fig. 2 a–e Measured plasma total radioactivity curves (expressed in SUV) in the test and retest scans in each subject; only the first 12 min after radiotracer injection are reported to emphasize the peak of each curve. SUV standard uptake value.

seven out of our 10 scans (Supplementary Material). Shortening the acquisition time without introduction of a < 5 % bias was deemed impossible in this dataset. Table 2 reports test-retest characteristics for V_T estimates obtained using shortened acquisitions. While overall average (across subjects, ROI by ROI) TRPD values remain in the range of ~ 7 to ~ 17 % for all approaches, the variability across subjects increases steadily with shorter scan durations. For all approaches, ICC values remain excellent (> 0.75) with shorter scan durations only in a subset of ROIs (gray matter cerebellum, medial and dorsolateral PFC, and dorsal putamen), and drop to below acceptable (< 0.5) in thalamus and hippocampus.

Noninvasive Estimation of Input Function

SIME provided input functions that were similar to the measured blood-based curves. The analysis based on arterial input function did not show significant difference between 1TC and 2TC in describing the TACs or in test-retest performance. Therefore, we report here the comparison between arterial blood-based and SIME-based estimates only using the more parsimonious of the two model configurations, the 1TC. Using SIME-derived input functions and 1TC resulted in V_T estimates that were highly correlated with, and numerically close to, those obtained using arterial input function (Fig. 6a, $r = 0.951$, slope $= 1.073$, intercept $= -1.037$). The optimal blood
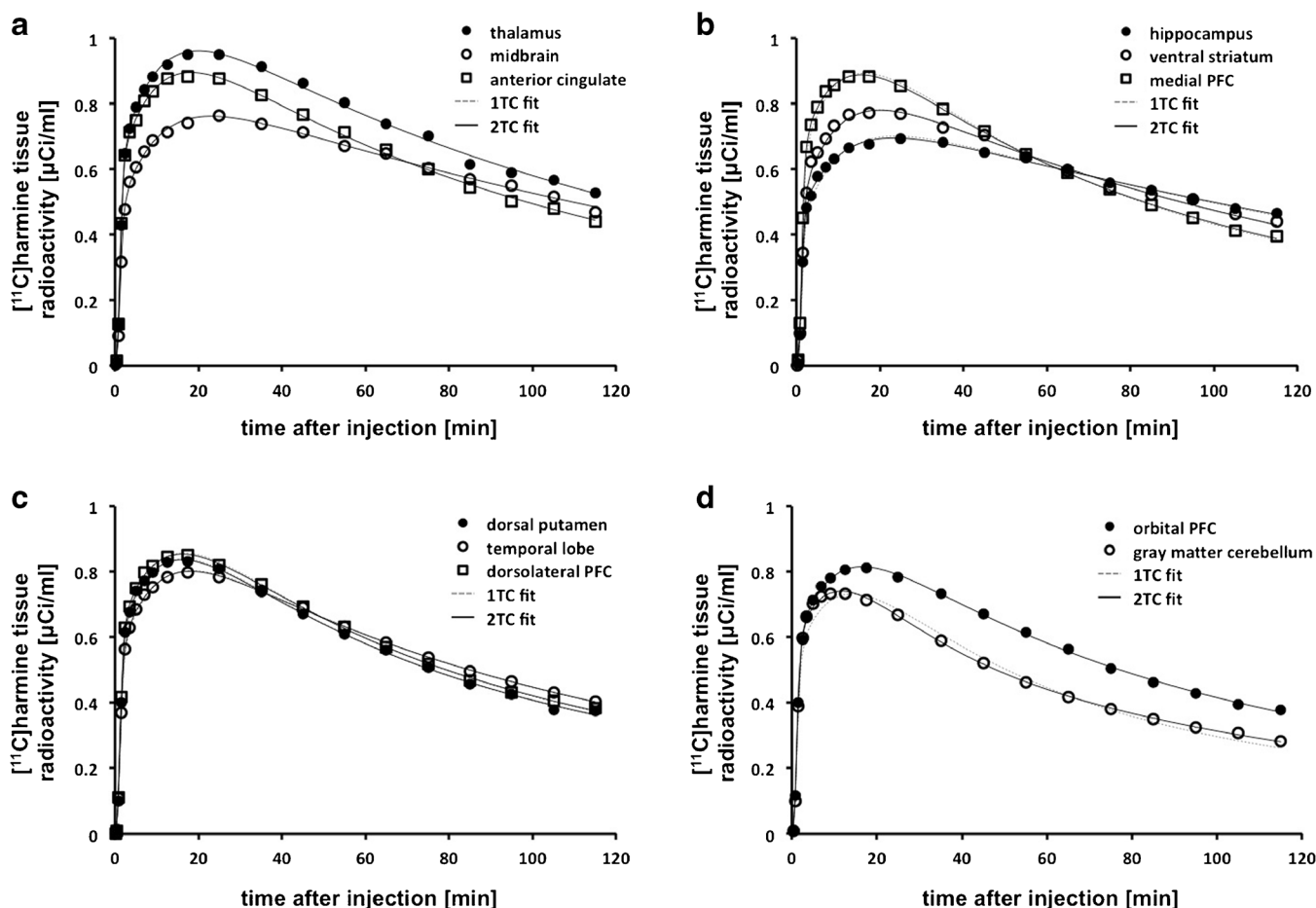
Fig. 3 **a–d** Time activity curves obtained for 11 regions in a representative subject (subject 3, test scan) are fit with a 1TC model (dashed line) and 2TC model (solid line). PFC prefrontal cortex, 1TC one-tissue compartment model, 2TC two-tissue compartment model.

sampling time was found to be 20 min post-injection. Note that V_T estimates obtained *via* SIME used TACs that were not corrected for vascular contribution, as this would be the case in absence of blood data. Results of similar regression analyses, conducted region by region, yielded a range of correlation values from 0.939 to 0.962, a range of slope values from 1.112 to 1.199, and a range of intercept values from −4.346 to −0.592. Paired two-tail t test, region by region, revealed no statistically significant differences between blood-based and SIME-based V_T estimates in our limited sample size dataset. Table 3 reports the percent difference values between blood-based and SIME-derived V_T estimates.

Compared to when using measured arterial input function, V_T estimated with SIME-derived input function showed numerically higher test-retest variability, with an average (across subjects) absolute test-retest difference in the range 16.6 to 22.0 % across ROIs (Fig. 6b). Paired two-tail t-test region by region revealed no significant difference between TRPD values obtained with blood-based 1TC and those obtained with SIME-based 1TC in this small size sample. Percent difference in the estimation of V_T was on average consistently higher for the retest scans than for the

test scans (Table 3), which could explain the higher test-retest variability when using SIME.

Overall, poor ICC values were obtained for V_T estimated using SIME-derived input function and 1TC (in the range 0.30 to 0.57 across ROIs) (Fig. 6c). Values were consistently lower than those for blood-based estimates.

Non-displaceable Distribution Volume and Specific Binding Potentials

Table 4 reports average estimates of V_{ND} and BP_P parameters quantified directly from the 2TC model kinetic rates, as well as test-retest characteristics for BP_P. Overall, estimates for V_{ND} were variable across regions, and estimates for BP_P showed higher test-retest variability than V_T in all ROI, and lower ICC scores, with the exception of thalamus, hippocampus, and orbital PFC.

Discussion

We present here the first systematic assessment of [11C]harmine test-retest repeatability for quantifying *in vivo* MAO-A binding
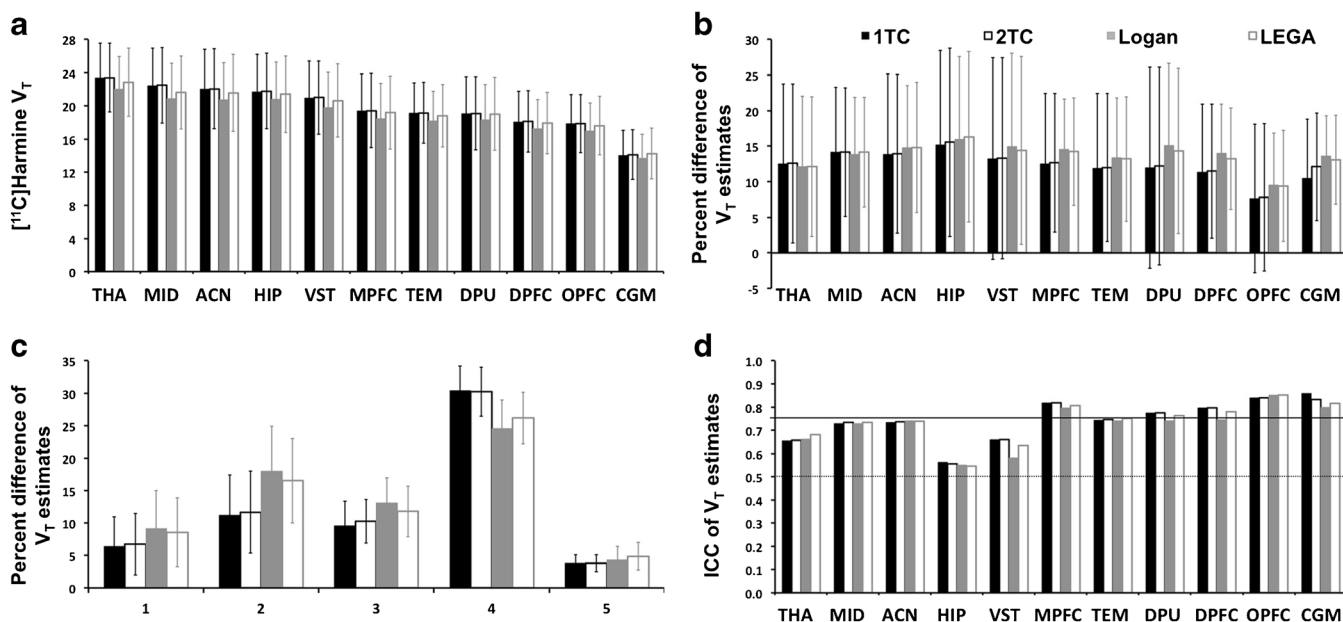
Fig. 4 **a** Average estimates of total distribution volume (V_T) obtained across considered regions and quantification methods; error bars reflect standard deviation (SD). **b** TRPD values obtained for total distribution volume (V_T) estimates; average values across subjects, region by region. **c** TRPD values obtained for total distribution volume (V_T) estimates: average values across regions, for the five subject. Error bars reflect standard deviation (SD). **d** ICC values obtained for total distribution volume (V_T) estimates; horizontal lines indicate the ICC = 0.5 (black dotted line) and ICC = 0.75 (black solid line) levels. 1TC, one-tissue compartment model; 2TC, two-tissue compartment model; Logan, Logan graphical analysis; LEGA, likelihood estimation in graphical analysis; PFC, prefrontal cortex; TRPD, test-retest percent difference. THA thalamus, MID midbrain, ACN anterior cingulate, HIP hippocampus, VST ventral striatum, MPFC medial prefrontal cortex, TEM temporal lobe, DPU dorsal putamen, DPFC dorsolateral prefrontal cortex, OPFC orbital prefrontal cortex, CGM cerebellar gray matter

in humans. We evaluated performances of various quantification strategies based on goodness of fit, identifiability and time stability, as well as test-retest metrics (absolute TRPD and ICC). With regard to test-retest properties, the results observed are comparable to those reported using other PET radiotracers [32, 44, 46, 47]. We further demonstrate the potential for a less-invasive estimation of input function *via* SIME, with respect to binding estimates and their repeatability.x

Regional Distribution Volume and Goodness of Fit

V_T values obtained here are consistent with earlier studies using [^{11}C]harmine [6, 16–19, 21–23, 48, 49]. The 1TC and 2TC models perform comparably with regard to goodness of fit, as assessed by WRSS and AIC comparison. Previous authors found that the 2TC model fits the data better than 1TC [23]. This is not consistent with our analysis, showing that the 2TC model performs as well as 1TC in all considered metrics. V_T values obtained with 1TC and 2TC models were overall not different from those estimated with Logan and LEGA, although a slight underestimation of Logan-based V_T compared to those obtained with 1TC was observed (slope = 0.922). It has been shown that, in the presence of noise, Logan is prone to inducing a negative bias [50]. LEGA, designed to decrease this

bias [40], provided estimates of V_T closer to those obtained by 1TC (slope = 0.962).

Test-Retest Repeatability

The 1TC and 2TC models performed similarly with regard to test-retest difference, ICC, and identifiability. The range of average TRPD values obtained across ROIs (7.7–15.6 %), using either 1TC and 2TC, is comparable to that reported for other PET radiotracers, such as [^{11}C]DASB (17–21 % [44]), [^{11}C]CUMI-101 (10–15 % [32]), [^{11}C]PBR28 (17 % [46]), and [^{11}C]LY2795050 (< 12 % [47]). Both 1TC and 2TC models resulted in acceptable to excellent ICC values across ROIs. The 1TC model overall performs the best in terms of TRPD, while 2TC shows a slightly better identifiability in the majority of considered ROIs.

Logan and LEGA perform somewhat similarly, although LEGA yields overall slightly lower TRPD values, higher ICC values, and better identifiability. ICC values obtained for both graphical methods are acceptable to excellent across ROIs. None of the two graphical methods perform quite as well as the compartment models, with exception of identifiability for LEGA, which is the best across methods in the majority of ROIs. However, no statistically significant differences are observed in our sample across performance indices in between kinetic models and graphical approaches.
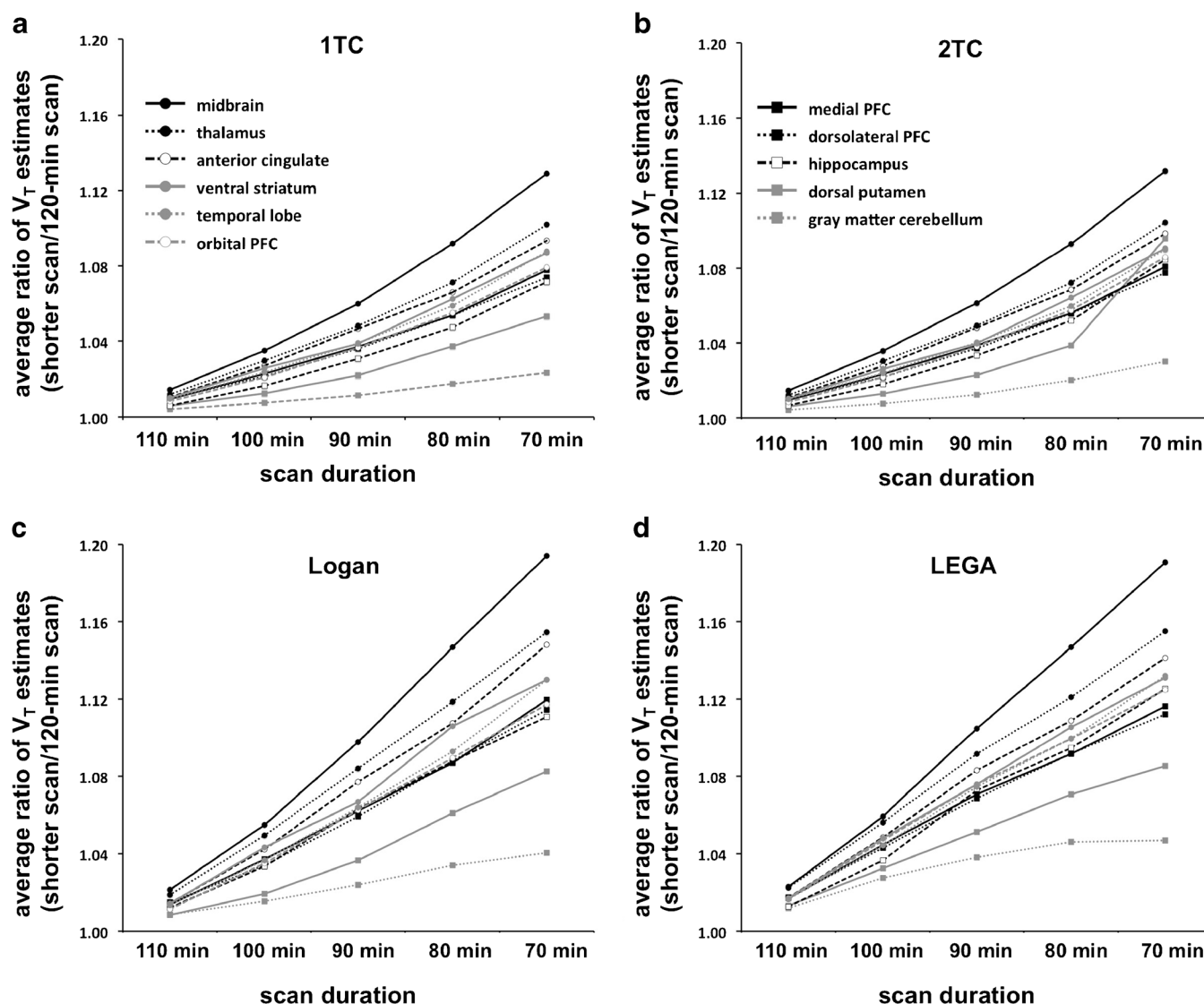
Fig. 5 Time stability: average (across scans) ratios between V_T obtained using a shortened acquisition and V_T obtained from the 120 min scan. **a** 1TC, one-tissue compartment model; **b** 2TC, two-tissue compartment model; **c** Logan graphical analysis; **d** LEGA, likelihood estimation in graphical analysis; PFC, prefrontal cortex; V_T, total distribution volume.

As the observed repeatability is consistent with that of other radiotracers and fairly stable across quantification procedure, we conclude that this tracer is useful to study the MAO-A role in neuropsychiatric or neurological conditions, either cross-sectionally or longitudinally.

Minimally Invasive Estimation

Given the risk and cost of arterial catheterization, being able to quantify [¹¹C]harmine binding without full arterial blood sampling would facilitate clinical studies with this radio-tracer. In our sample, SIME led to V_T estimates that highly correlate with, and are numerically close to, those obtained from arterial catheterization, with no statistically significant difference between blood-based and SIME-based V_T estimates. Thus, simplifying acquisition of [¹¹C]harmine data

may be possible by eliminating arterial catheterization, provided that accurate sampling of one arterial blood sample at 20 min post-injection, and parent fraction analysis on such sample can be reliably obtained. SIME-based estimates will be highly dependent on the accuracy of this measurement. However, SIME could also rely on a few blood samples obtained at different time points, so that the sensitivity towards measurement errors would be reduced. Future studies should investigate whether it is possible to substitute arterial with venous blood for such quantification.

Using SIME to estimate V_T did not excessively compromise test-retest repeatability of measurements compared to using full arterial sampling (paired sample t-test did not reach significance). However, this is a small sample size dataset, and the range of average TRPD values obtained for [¹¹C]harmine V_T across ROIs using 1TC increases to 16.6 to 22.0 % with SIME.

Table 2. Test-retest properties of V_T measurements obtained with shorter scans. TRPD and ICC values (average ± SD) obtained for total distribution volume (V_T) estimates obtained using a shortened acquisition; average values across subjects, region by region, are reported for TRPD. *1TC* one-tissue compartment model, *2TC* two-tissue compartment model, *Logan* Logan graphical analysis, *LEGA* likelihood estimation in graphical analysis, *TRPD* test-retest percent difference, *ICC* intraclass correlation coefficient, *THA* thalamus, *MID* midbrain, *ACN* anterior cingulate, *HIP* hippocampus, *VST* ventral striatum, *MPFC* medial prefrontal cortex, *TEM* temporal lobe, *DPU* dorsal putamen, *DPFC* dorsolateral prefrontal cortex, *OPFC* orbital prefrontal cortex, *CGM* cerebellar gray matter, *SD* standard deviation

Region	TRPD					ICC				
	110 min	100 min	90 min	80 min	70 min	110 min	100 min	90 min	80 min	70 min
1TC										
THA	12.8 ± 11.6	13.2 ± 13.8	13.8 ± 15.5	14.4 ± 16.5	14.7 ± 18.0	0.63	0.57	0.52	0.46	0.37
MID	15.2 ± 10.3	14.6 ± 10.9	13.7 ± 12.8	14.5 ± 15.3	15.8 ± 17.6	0.69	0.71	0.70	0.63	0.49
ACN	13.6 ± 11.8	13.3 ± 13.3	13.4 ± 14.5	13.4 ± 15.7	13.1 ± 18.3	0.72	0.71	0.68	0.67	0.63
HIP	14.5 ± 14.4	13.9 ± 15.3	14.5 ± 16.6	14.8 ± 18.9	14.2 ± 19.8	0.57	0.57	0.52	0.44	0.39
VST	12.8 ± 14.8	13.8 ± 17.8	13.8 ± 19.1	12.4 ± 20.0	12.3 ± 20.8	0.68	0.57	0.54	0.60	0.56
MPFC	12.0 ± 10.9	11.6 ± 12.4	10.6 ± 13.1	10.7 ± 15.1	11.2 ± 16.8	0.81	0.80	0.80	0.77	0.73
TEM	11.4 ± 11.4	11.1 ± 12.3	10.6 ± 13.3	10.7 ± 14.8	11.5 ± 15.3	0.74	0.72	0.71	0.68	0.62
DPU	11.3 ± 14.1	11.0 ± 15.5	11.2 ± 16.4	12.3 ± 15.5	13.3 ± 15.8	0.78	0.77	0.75	0.76	0.74
DPFC	10.4 ± 10.5	9.9 ± 11.5	9.4 ± 12.7	9.6 ± 14.3	10.5 ± 15.5	0.81	0.80	0.78	0.75	0.71
OPFC	7.9 ± 11.4	8.7 ± 12.0	10.1 ± 11.8	11.6 ± 11.8	13.8 ± 12.5	0.82	0.79	0.77	0.73	0.66
CGM	9.9 ± 9.0	9.2 ± 9.6	8.5 ± 10.7	8.5 ± 12.3	7.6 ± 12.8	0.87	0.87	0.87	0.85	0.85
2TC										
THA	12.9 ± 11.6	13.4 ± 13.7	14.0 ± 15.4	14.6 ± 16.2	15.0 ± 17.9	0.63	0.57	0.53	0.48	0.39
MID	15.3 ± 10.3	14.7 ± 10.8	13.7 ± 12.7	14.6 ± 14.9	15.6 ± 17.9	0.69	0.71	0.71	0.65	0.50
ACN	13.7 ± 11.8	13.5 ± 13.3	13.6 ± 14.4	13.6 ± 15.4	13.7 ± 18.0	0.72	0.71	0.69	0.68	0.62
HIP	14.9 ± 14.5	14.4 ± 15.2	15.2 ± 16.5	15.6 ± 18.5	16.1 ± 18.8	0.56	0.56	0.51	0.44	0.36
VST	13.0 ± 14.8	14.0 ± 17.8	13.9 ± 19.0	12.5 ± 19.8	12.6 ± 20.7	0.68	0.57	0.54	0.61	0.57
MPFC	12.2 ± 10.7	11.9 ± 12.2	10.9 ± 12.8	11.0 ± 14.8	11.2 ± 16.9	0.81	0.80	0.80	0.77	0.73
TEM	11.5 ± 11.3	11.2 ± 12.3	10.9 ± 13.2	10.8 ± 14.6	11.3 ± 15.6	0.74	0.72	0.71	0.69	0.63
DPU	11.6 ± 13.9	11.1 ± 15.5	11.1 ± 16.4	12.1 ± 15.6	19.6 ± 19.3	0.78	0.76	0.75	0.77	0.47
DPFC	10.5 ± 10.4	10.1 ± 11.4	9.6 ± 12.6	9.6 ± 14.2	10.6 ± 15.5	0.81	0.80	0.78	0.76	0.71
OPFC	8.0 ± 11.3	8.7 ± 12.0	10.1 ± 11.7	11.8 ± 11.6	14.6 ± 12.2	0.82	0.79	0.77	0.73	0.64
CGM	11.4 ± 8.2	10.5 ± 8.9	9.8 ± 10.0	9.9 ± 11.4	9.3 ± 11.8	0.84	0.85	0.86	0.84	0.84
Logan										
THA	12.5 ± 9.2	12.9 ± 11.8	14.0 ± 14.5	14.7 ± 15.2	14.9 ± 17.5	0.66	0.61	0.53	0.49	0.40
MID	16.3 ± 8.8	14.9 ± 8.6	13.4 ± 10.7	14.4 ± 13.3	16.4 ± 17.4	0.66	0.72	0.73	0.66	0.47
ACN	14.6 ± 9.3	14.0 ± 11.6	14.4 ± 13.1	13.9 ± 14.4	13.4 ± 17.7	0.72	0.72	0.67	0.68	0.64
HIP	15.1 ± 13.6	14.3 ± 14.2	15.7 ± 15.6	15.9 ± 18.4	15.1 ± 18.7	0.56	0.60	0.51	0.42	0.40
VST	12.9 ± 12.2	15.0 ± 16.6	15.6 ± 18.2	13.1 ± 19.1	13.7 ± 20.0	0.71	0.53	0.47	0.60	0.56
MPFC	13.5 ± 8.2	12.9 ± 10.6	11.2 ± 11.5	11.2 ± 14.0	11.3 ± 16.9	0.81	0.80	0.81	0.77	0.73
TEM	12.6 ± 9.6	11.9 ± 10.8	11.3 ± 12.1	11.1 ± 13.8	11.4 ± 15.5	0.74	0.73	0.72	0.69	0.63
DPU	13.5 ± 10.8	12.5 ± 13.8	12.1 ± 15.7	12.3 ± 15.0	13.5 ± 15.4	0.77	0.76	0.73	0.77	0.74
DPFC	11.8 ± 7.8	11.0 ± 9.3	10.3 ± 11.1	9.4 ± 13.7	10.6 ± 15.5	0.81	0.81	0.79	0.76	0.71
OPFC	8.9 ± 9.2	8.6 ± 11.0	9.4 ± 11.6	11.4 ± 11.0	13.8 ± 12.5	0.84	0.81	0.78	0.75	0.67
CGM	12.2 ± 6.8	10.6 ± 7.8	9.4 ± 9.7	9.3 ± 12.2	8.4 ± 12.9	0.83	0.85	0.86	0.83	0.84
LEGA										
THA	12.4 ± 9.6	13.2 ± 12.0	14.1 ± 14.3	15.0 ± 15.3	15.2 ± 16.9	0.69	0.63	0.55	0.48	0.39
MID	15.5 ± 8.5	14.4 ± 8.8	13.4 ± 10.8	14.7 ± 13.5	15.7 ± 16.2	0.70	0.73	0.72	0.64	0.49
ACN	14.4 ± 10.1	14.1 ± 12.7	14.3 ± 14.1	14.3 ± 15.5	13.7 ± 18.0	0.73	0.71	0.67	0.65	0.62
HIP	15.1 ± 14.1	14.6 ± 15.1	15.7 ± 16.4	16.2 ± 18.8	15.6 ± 19.3	0.57	0.58	0.51	0.42	0.37
VST	12.8 ± 14.0	14.1 ± 16.7	14.3 ± 18.1	13.0 ± 19.0	12.8 ± 19.6	0.70	0.59	0.54	0.62	0.59
MPFC	13.0 ± 8.9	12.6 ± 11.4	11.4 ± 12.5	11.6 ± 15.0	11.5 ± 17.0	0.82	0.80	0.80	0.76	0.72
TEM	12.2 ± 9.9	11.7 ± 11.4	11.2 ± 12.6	11.2 ± 14.5	11.6 ± 15.2	0.76	0.74	0.72	0.68	0.63
DPU	12.5 ± 11.9	11.6 ± 14.9	11.9 ± 16.1	13.0 ± 15.6	14.1 ± 15.8	0.79	0.77	0.74	0.75	0.72
DPFC	11.3 ± 8.4	10.8 ± 10.4	10.2 ± 12.1	9.9 ± 14.5	10.8 ± 15.5	0.82	0.81	0.78	0.74	0.70
OPFC	8.3 ± 9.7	8.6 ± 11.4	10.3 ± 11.3	12.4 ± 11.3	14.9 ± 12.1	0.85	0.81	0.77	0.72	0.63
CGM	11.5 ± 7.5	10.2 ± 9.1	9.3 ± 10.6	9.4 ± 12.7	8.7 ± 12.9	0.85	0.85	0.85	0.83	0.83

Furthermore, ICC values are overall poorer when using 1TC and SIME, as compared to blood-based analysis. It is possible that, in a larger sample, V_T obtained using full arterial blood sampling would have resulted in significantly better test-retest reproducibility.

SIME is based on the idea that information about the shape of the metabolite-corrected arterial input function, which is assumed by all methods to be common across brain regions, is implicitly contained in the tissue TACs, and that by simultaneous modeling of these TACs, SIME is able to identify the input function shape. SIME does not assume a fixed shape for the arterial input function across subjects or across conditions. Theoretically, SIME should therefore be able to identify a reasonable estimate of the arterial input function in controls, patients, and individuals under treatment conditions, as long as a subject-specific 20 min arterial sample is available. However, we emphasize the importance of explicitly evaluating SIME under the relevant conditions before being used systematically in clinical studies.
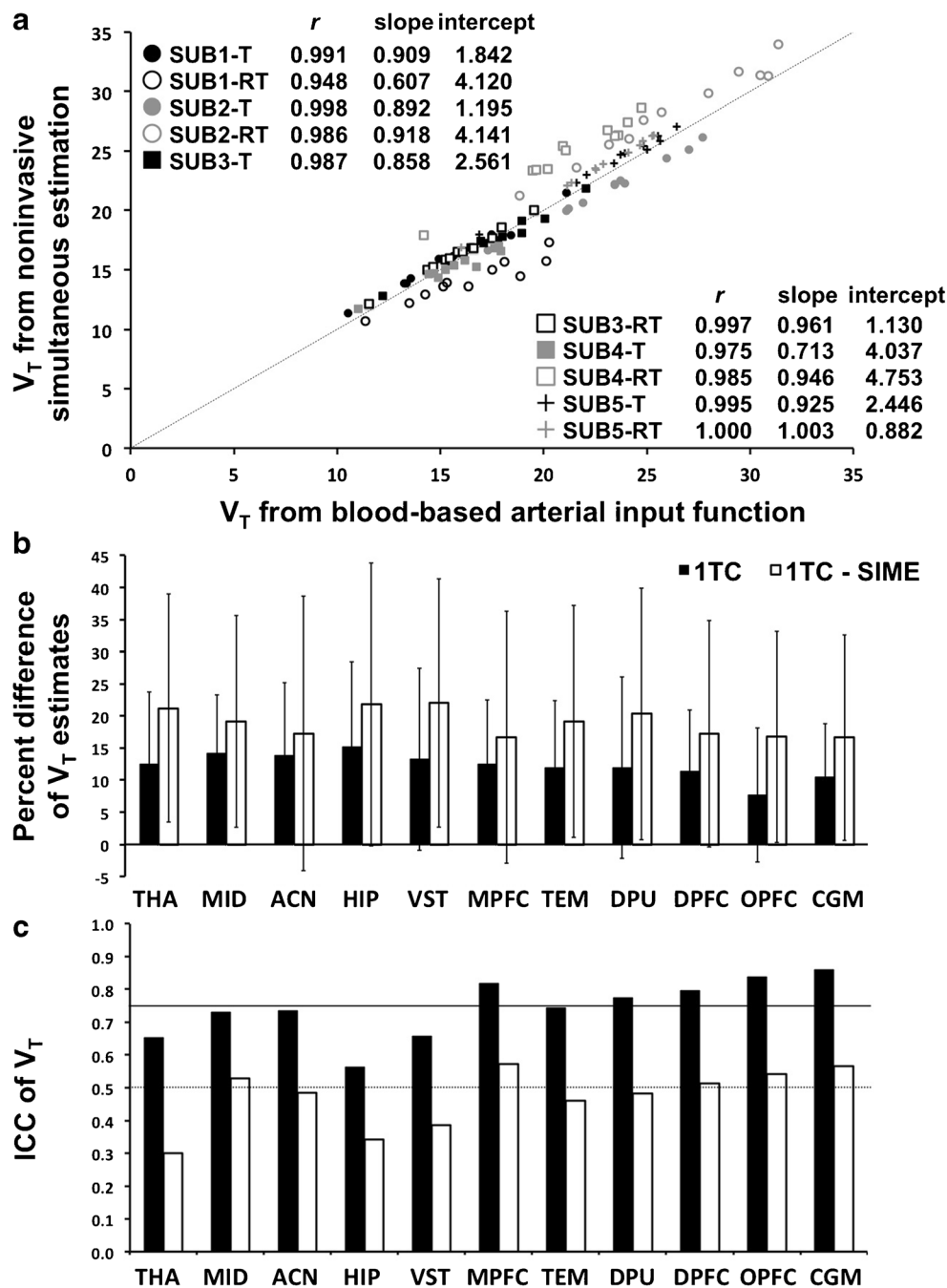
Fig. 6 **a** Scatter plot of V_T values obtained using measured arterial input function (*x*-axis) and SIME-derived input function (*y*-axis) using the 1TC model. The black dotted line indicates the identity line. **b** TRPD values obtained for total distribution volume (V_T) estimates using SIME (average values across subjects, region by region). Error bars reflect standard deviation (SD). **c** ICC values obtained for total distribution volume (V_T) estimates using SIME-derived input function; horizontal lines indicate the ICC = 0.5 (black dotted line) and ICC = 0.75 (black solid line) levels. 1TC, one-tissue compartment model; PFC, prefrontal cortex; SIME, simultaneous estimation; V_T, total distribution volume; TRPD, test-retest percent difference. THA thalamus, MID midbrain, ACN anterior cingulate, HIP hippocampus, VST ventral striatum, MPFC medial prefrontal cortex, TEM temporal lobe, DPU dorsal putamen, DPFC dorsolateral prefrontal cortex, OPFC orbital prefrontal cortex, CGM cerebellar gray matter

Non-Displaceable and Specific Binding

In absence of a reference region, estimation of [^{11}C]harmine V_{ND} and binding potentials remains a challenge. Direct estimation of these entities from kinetic rates showed poor identifiability and thus large uncertainty, similar to a previous report [39]. For instance, TRPD was lower than 20 % only in thalamus, and ICC only reached acceptable levels in thalamus, dorsal putamen, and dorsolateral and orbital PFC. We therefore do not recommend these procedures. The outcome measure of

Table 3. Simultaneous estimation of input function. Percent difference between blood-based V_T estimates and SIME-derived V_T estimates, using 1TC. V_T total distribution volume, *1TC* one-tissue compartment model, *THA* thalamus, *MID* midbrain, *ACN* anterior cingulate, *HIP* hippocampus, *VST* ventral striatum, *MPFC* medial prefrontal cortex, *TEM* temporal lobe, *DPU* dorsal putamen, *DPFC* dorsolateral prefrontal cortex, *OPFC* orbital prefrontal cortex, *CGM* cerebellar gray matter, *SD* standard deviation

	SUB 1 T	SUB 1 RT	SUB 2 T	SUB 2 RT	SUB 3 T	SUB 3 RT	SUB 4 T	SUB 4 RT	SUB 5 T	SUB 5 RT
THA	1.77	14.70	5.64	8.28	0.88	2.38	4.39	13.79	2.88	4.12
MID	2.56	21.82	7.14	2.79	3.80	1.31	7.60	11.48	0.83	3.41
ACN	3.42	13.60	6.08	7.47	0.88	3.27	4.77	15.78	2.23	3.92
HIP	1.74	23.36	7.08	1.45	4.49	0.98	8.92	12.03	0.44	3.22
VST	2.86	14.29	5.26	6.74	0.96	2.83	2.46	15.84	2.42	3.92
MPFC	3.63	10.21	5.48	9.85	2.85	4.12	1.84	18.85	3.72	4.40
TEM	1.68	16.69	5.77	7.98	0.75	3.39	3.80	16.25	2.47	4.05
DPU	6.86	9.27	4.98	11.07	2.93	4.34	1.41	21.46	4.16	4.68
DPFC	4.71	9.13	4.79	10.24	2.74	4.09	0.32	20.10	4.15	4.63
OPFC	5.46	9.46	5.28	9.32	2.30	3.93	1.30	19.30	3.52	4.56
CGM	7.93	5.71	3.66	12.82	5.21	5.68	6.56	26.01	6.62	5.58
Average	3.87	13.48	5.56	8.00	2.53	3.30	3.94	17.35	3.04	4.23
SD	2.13	5.51	0.99	3.39	1.55	1.37	2.81	4.32	1.71	0.65

choice for [¹¹C]harmine is V_T. We have previously proposed a method that estimates V_{ND} in absence of a reference region [29]. However, application of this procedure to [¹¹C]harmine consistently failed to provide a unique solution.

Limitations

There is an absence of females in our study population. There is evidence from animal and human studies of interactions between sex hormones and neurotransmitters [51]. MAO-A mRNA and activity are decreased after estrogen treatment [52], higher brain MAO-A levels are found during the first week postpartum compared to women who had not recently been pregnant [19], and higher MAO-A binding has been shown in prefrontal cortex during perimenopausal transition phase, compared with age-matched women during reproductive years and menopause [53]. The menstrual cycle influences could lower test-retest

Table 4. Non-displaceable and specific binding: values, TRPD, and ICC. Estimates of V_{ND} and BP_P and values of test-retest percent difference and ICC for BP_P, obtained across regions. Average ± SD (across subjects) estimates are reported for V_{ND}, BP_P, and TRPD values. *2TC* two-tissue compartment model, V_{ND} non-displaceable distribution volume, BP_P specific binding potential, *PFC* prefrontal cortex, *SD* standard deviation, *TRPD* test-retest percent difference

Region	V_{ND}	BP_P	BP_P TRPD	BP_P ICC
Thalamus	2.75 ± 3.70	20.66 ± 6.55	14.91 ± 11.96	0.85
Midbrain	6.08 ± 4.86	16.39 ± 7.27	42.83 ± 19.52	0.45
Anterior cingulate	3.71 ± 3.41	18.34 ± 7.87	40.90 ± 39.82	0.48
Hippocampus	3.03 ± 2.97	18.75 ± 6.06	27.25 ± 17.99	0.57
Ventral striatum	3.44 ± 3.81	17.56 ± 7.47	36.96 ± 48.38	0.39
Medial PFC	7.77 ± 5.17	11.65 ± 8.01	64.03 ± 33.83	0.41
Temporal lobe	3.37 ± 4.39	15.78 ± 6.81	36.02 ± 42.50	0.68
Dorsal putamen	4.42 ± 5.05	14.67 ± 7.95	50.37 ± 49.89	0.76
Dorsolateral PFC	5.24 ± 4.60	12.86 ± 7.31	47.86 ± 35.59	0.75
Orbital PFC	4.71 ± 4.53	13.14 ± 6.99	32.29 ± 34.78	0.85
Cerebellar gray matter	5.98 ± 4.64	8.11 ± 6.15	62.63 ± 49.12	0.61

repeatability; hence, confirmation of our findings in women would be desirable.

The last measure of parent fraction in plasma is acquired at 95 min post-injection. Although extrapolation of parent fraction values up to 120 min post-injection is based on fits obtained using a Hill function, which provided good fit of all parent fraction curves in the dataset (Fig. 1), this extrapolation may have an effect on the metabolite-corrected arterial input function, and thus on the reported time stability of the outcome measures.

Interpretation of findings should also take into account the small sample size.

Conclusions

We find the test-retest repeatability of [¹¹C]harmine binding to MAO-A, when quantified using arterial blood sampling and either 1TC and 2TC models, to be comparable to that of other used radiotracers, thus prospective and cross-sectional studies are possible using [¹¹C]harmine. Our results using SIME further suggest that simplifying acquisition of [¹¹C]harmine data by eliminating arterial catheterization may be possible, provided that accurate sampling of one arterial blood sample at 20 min post-injection, and parent fraction analysis on such sample, can be obtained. Quantification of [¹¹C]harmine binding potentials remains a challenge that requires further investigation.

Compliance with Ethical Standards

Conflicts of Interest

Drs. Zanderigo, D'Agostino, Schain, Kumar, Parsey, and Delorenzo, and Ms. Joshi declare no conflicts of interest. Dr. Mann receives royalties for commercial use of the Columbia-Suicide Severity Rating Scales from the Research Foundation for Mental Hygiene.

References

1. Weyler W, Hsu YP, Breakefield XO (1990) Biochemistry and genetics of monoamine oxidase. Pharmacol Ther 47(3):391–417. https://doi.org/10.1016/0163-7258(90)90064-9

2. Johnston JP (1968) Some observations upon a new inhibitor of monoamine oxidase in brain tissue. Biochem Pharmacol 17(7):1285–1297. https://doi.org/10.1016/0006-2952(68)90066-X

3. Shih JC, Chen K, Ridd MJ (1999) Monoamine oxidase: from genes to behavior. Annu Rev Neurosci 22(1):197–217. https://doi.org/10.1146/annurev.neuro.22.1.197

4. Youdim MB, Edmondson D, Tipton KF (2006) The therapeutic potential of monoamine oxidase inhibitors. Nat Rev Neurosci 7(4):295–309. https://doi.org/10.1038/nrn1883

5. Livingston MG, Livingston HM (1996) Monoamine oxidase inhibitors. An update on drug interactions. Drug Saf 14(4):219–227. https://doi.org/10.2165/00002018-199614040-00002

6. Meyer JH, Ginovart N, Boovariwala A, Sagrati S, Hussey D, Garcia A, Young T, Praschak-Rieder N, Wilson AA, Houle S (2006) Elevated monoamine oxidase a levels in the brain: an explanation for the monoamine imbalance of major depression. Arch Gen Psychiatry 63(11):1209–1216. https://doi.org/10.1001/archpsyc.63.11.1209

7. Ametamey SM, Beer HF, Guenther I, Antonini A, Leenders KL, Waldmeier PC, Schubiger PA (1996) Radiosynthesis of [^{11}C]brofaromine, a potential tracer for imaging monoamine oxidase a. Nucl Med Biol 23(3):229–234. https://doi.org/10.1016/0969-8051(95)02051-9

8. Bottlaender M, Dolle F, Guenther I, Roumenov D, Fuseau C, Bramoulle Y, Curet O, Jegham J, Pinquier JL, George P, Valette H (2003) Mapping the cerebral monoamine oxidase type A: positron emission tomography characterization of the reversible selective inhibitor [^{11}C]befloxatone. J Pharmacol Exp Ther 305(2):467–473. https://doi.org/10.1124/jpet.102.046953

9. Fowler JS, MacGregor RR, Wolf AP et al (1987) Mapping human brain monoamine oxidase A and B with 11C-labeled suicide inactivators and PET. Science 235(4787):481–485. https://doi.org/10.1126/science.3099392

10. Ohmomo Y, Hirata M, Murakami K et al (1991) Synthesis of fluorine and iodine analogues of clorgyline and selective inhibition of monoamine oxidase A. Chem Pharm Bull (Tokyo) 39(4):1038–1040. https://doi.org/10.1248/cpb.39.1038

11. Ohmomo Y, Hirata M, Murakami K et al (1993) Synthesis and characterization of 11C-labeled fluoroclorgyline: a monoamine oxidase A specific inhibitor for positron emission tomography. Chem Pharm Bull (Tokyo) 41(11):1994–1997. https://doi.org/10.1248/cpb.41.1994

12. Bergstrom M, Westerberg G, Kihlberg T, Langstrom B (1997) Synthesis of some 11C-labelled MAO-A inhibitors and their in vivo uptake kinetics in rhesus monkey brain. Nucl Med Biol 24(5):381–388. https://doi.org/10.1016/S0969-8051(97)80003-0

13. Bergstrom M, Westerberg G, Langstrom B (1997) ^{11}C-harmine as a tracer for monoamine oxidase A (MAO-A): in vitro and in vivo studies. Nucl Med Biol 24(4):287–293. https://doi.org/10.1016/S0969-8051(97)00013-9

14. Kim H, Sablin SO, Ramsay RR (1997) Inhibition of monoamine oxidase A by beta-carboline derivatives. Arch Biochem Biophys 337(1):137–142. https://doi.org/10.1006/abbi.1996.9771

15. Murthy R, Erlandsson K, Kumar D, van Heertum R, Mann J, Parsey R (2007) Biodistribution and radiation dosimetry of ^{11}Charmine in baboons. Nucl Med Commun 28(9):748–754. https://doi.org/10.1097/MNM.0b013e32827420b5

16. Chiuccariello L, Houle S, Miler L, Cooke RG, Rusjan PM, Rajkowska G, Levitan RD, Kish SJ, Kolla NJ, Ou X, Wilson AA, Meyer JH (2014) Elevated monoamine oxidase a binding during major depressive episodes is associated with greater severity and reversed neurovegetative symptoms. Neuropsychopharmacology 39(4):973–980. https://doi.org/10.1038/npp.2013.297

17. Meyer JH, Wilson AA, Sagrati S, Miler L, Rusjan P, Bloomfield PM, Clark M, Sacher J, Voineskos AN, Houle S (2009) Brain monoamine oxidase A binding in major depressive disorder: relationship to selective serotonin reuptake inhibitor treatment, recovery, and recurrence. Arch Gen Psych 66(12):1304–1312. https://doi.org/10.1001/archgenpsychiatry.2009.156

18. Sacher J, Houle S, Parkes J, Rusjan P, Sagrati S, Wilson AA, Meyer JH (2011) Monoamine oxidase A inhibitor occupancy during treatment of major depressive episodes with moclobemide or St. John's wort: an [^{11}C]-harmine PET study. J Psychiatry Neurosci 36(6):375–382. https://doi.org/10.1503/jpn.100117

19. Sacher J, Wilson AA, Houle S, Rusjan P, Hassan S, Bloomfield PM, Stewart d, Meyer JH (2010) Elevated brain monoamine oxidase A binding in the early postpartum period. Arch Gen Psych 67(5):468–474. https://doi.org/10.1001/archgenpsychiatry.2010.32

20. Sacher J, Rabiner EA, Clark M, Rusjan P, Soliman A, Boskovic R, Kish SJ, Wilson AA, Houle S, Meyer JH (2012) Dynamic, adaptive changes in MAO-A binding after alterations in substrate availability: an in vivo [^{11}C]-harmine positron emission tomography study. J Cereb Blood Flow Metabolism 32(3):443–446. https://doi.org/10.1038/jcbfm.2011.184

21. Kolla NJ, Matthews B, Wilson AA, Houle S, Michael Bagby R, Links P, Simpson AI, Hussain A, Meyer JH (2015) Lower monoamine oxidase-A total distribution volume in impulsive and violent male offenders with antisocial personality disorder and high psychopathic traits: an [^{11}C] Harmine positron emission tomography study. Neuropsychopharmacology 40(11):2596–2603. https://doi.org/10.1038/npp.2015.106

22. Kolla NJ, Chiuccariello L, Wilson AA, Houle S, Links P, Bagby RM, McMain S, Kellow C, Patel J, Rekkas PV, Pasricha S, Meyer JH (2016) Elevated monoamine oxidase-a distribution volume in borderline personality disorder is associated with severity across mood symptoms, suicidality, and cognition. Biol Psych 79(2):117–126. https://doi.org/10.1016/j.biopsych.2014.11.024

23. Ginovart N, Meyer JH, Boovariwala A, Hussey D, Rabiner EA, Houle S, Wilson AA (2006) Positron emission tomography quantification of [^{11}C]-harmine binding to monoamine oxidase-A in the human brain. J Cereb Blood Flow Metabolism 26(3):330–344. https://doi.org/10.1038/sj.jcbfm.9600197

24. Gunn RN, Gunn SR, Cunningham VJ (2001) Positron emission tomography compartmental models. J Cereb Blood Flow Metab 21(6):635–652. https://doi.org/10.1097/00004647-200106000-00002

25. Logan J, Fowler JS, Volkow ND, Wolf AP, Dewey SL, Schlyer DJ, MacGregor RR, Hitzemann R, Bendriem B, Gatley SJ, Christman DR (1990) Graphical analysis of reversible radioligand binding from time-activity measurements applied to [N-^{11}C-methyl]-(-)-cocaine PET studies in human subjects. J Cereb Blood Flow Metab 10(5):740–747. https://doi.org/10.1038/jcbfm.1990.127

26. Innis RB, Cunningham VJ, Delforge J, Fujita M, Gjedde A, Gunn RN, Holden J, Houle S, Huang SC, Ichise M, Iida H, Ito H, Kimura Y, Koeppe RA, Knudsen GM, Knuuti J, Lammertsma AA, Laruelle M, Logan J, Maguire RP, Mintun MA, Morris ED, Parsey R, Price JC, Slifstein M, Sossi V, Suhara T, Votaw JR, Wong DF, Carson RE (2007) Consensus nomenclature for in vivo imaging of reversibly binding radioligands. J Cereb Blood Flow Metab 27(9):1533–1539. https://doi.org/10.1038/sj.jcbfm.9600493

27. Saura J, Kettler R, Da Prada M, Richards JG (1992) Quantitative enzyme radioautography with ^{3}H-Ro 41-1049 and ^{3}H-Ro 19-6327 in vitro: localization and abundance of MAO-A and MAO-B in rat CNS, peripheral organs, and human brain. J Neurosci 12(5):1977–1999

28. Saura J, Bleuel Z, Ulrich J, Mendelowitsch A, Chen K, Shih JC, Malherbe P, da Prada M, Richards JG (1996) Molecular neuroanatomy of human monoamine oxidases a and B revealed by quantitative enzyme radioautography and in situ hybridization histochemistry. Neuroscience 70(3):755–774. https://doi.org/10.1016/S0306-4522(96)83013-2

29. Todd Ogden R, Zanderigo F, Parsey RV (2015) Estimation of in vivo nonspecific binding in positron emission tomography studies without requiring a reference region. NeuroImage 108:234–242. https://doi.org/10.1016/j.neuroimage.2014.12.038

30. First MB, Spitzer RL, Gibbon M, Williams JB (2012) Structured Clinical Interview for DSM-IV® Axis I Disorders (SCID-I), Clinician Version, : American Psychiatric Pub

31. Avants BB, Tustison NJ, Wu J, Cook PA, Gee JC (2011) An open source multivariate framework for n-tissue segmentation with evaluation on public data. Neuroinformatics 9(4):381–400. https://doi.org/10.1007/s12021-011-9109-y

32. Milak MS, DeLorenzo C, Zanderigo F, Prabhakaran J, Kumar JSD, Majo VJ, Mann JJ, Parsey RV (2010) In vivo quantification of human serotonin

1A receptor using ¹¹C-CUMI-101, an agonist PET radiotracer. J Nucl Med 51(12):1892–1900. https://doi.org/10.2967/jnumed.110.076257

33. Shattuck DW, Mirza M, Adisetiyo V, Hojatkashani C, Salamon G, Narr KL, Poldrack RA, Bilder RM, Toga AW (2008) Construction of a 3D probabilistic atlas of human cortical structures. NeuroImage 39(3):1064–1080. https://doi.org/10.1016/j.neuroimage.2007.09.031

34. Gunn RN, Sargent PA, Bench CJ, Rabiner EA, Osman S, Pike VW, Hume SP, Grasby PM, Lammertsma AA (1998) Tracer kinetic modeling of the 5-HT1A receptor ligand [carbonyl-¹¹C]WAY-100635 for PET. NeuroImage 8(4):426–440. https://doi.org/10.1006/nimg.1998.0379

35. Parsey RV, Ojha A, Ogden RT, Erlandsson K, Kumar D, Landgrebe M, van Heertum R, Mann JJ (2006) Metabolite considerations in the in vivo quantification of serotonin transporters using ¹¹C-DASB and PET in humans. J Nucl Med 47(11):1796–1802

36. Parsey RV, Slifstein M, Hwang DR, Abi-Dargham A, Simpson N, Mawlawi O, Guo NN, van Heertum R, Mann JJ, Laruelle M (2000) Validation and reproducibility of measurement of 5-HT1A receptor parameters with [carbonyl-¹¹C]WAY-100635 in humans: comparison of arterial and reference tissue input functions. J Cereb Blood Flow Metab 20(7):1111–1133. https://doi.org/10.1097/00004647-200007000-00011

37. Watson CC, Newport D, Casey ME (1996) A single scatter simulation technique for scatter correction in 3D PET. In: Grangeat P, Amans JL (eds) Three-dimensional image reconstruction in radiology and nuclear medicine. Computational imaging and vision, vol 4. Springer, Dordrecht. https://doi.org/10.1007/978-94-015-8749-5_18

38. Mawlawi O, Martinez D, Slifstein M, Broft A, Chatterjee R, Hwang DR, Huang Y, Simpson N, Ngo K, van Heertum R, Laruelle M (2001) Imaging human mesolimbic dopamine transmission with positron emission tomography: I. Accuracy and precision of D(2) receptor parameter measurements in ventral striatum. J Cereb Blood Flow Metab 21(9):1034–1057. https://doi.org/10.1097/00004647-200109000-00002

39. Slifstein M, Laruelle M (2001) Models and methods for derivation of in vivo neuroreceptor parameters with PET and SPECT reversible radiotracers. Nucl Med Biol 28(5):595–608. https://doi.org/10.1016/S0969-8051(01)00214-1

40. Ogden RT (2003) Estimation of kinetic parameters in graphical analysis of PET imaging data. Statistics Med 22(22):3557–3568. https://doi.org/10.1002/sim.1562

41. Akaike H (1974) A new look at the statistical model identification. IEEE Trans Automat Contr AC-19(6):716–23. https://doi.org/10.1109/TAC.1974.1100705

42. Rosario BL, Weissfeld LA, Laymon CM, Mathis CA, Klunk WE, Berginc MD, James JA, Hoge JA, Price JC (2011) Inter-rater reliability of manual and automated region-of-interest delineation for PiB PET. NeuroImage 55(3):933–941. https://doi.org/10.1016/j.neuroimage.2010.12.070

43. Ogden RT, Tarpey T (2006) Estimation in regression models with externally estimated parameters. Biostatistics 7(1):115–129. https://doi.org/10.1093/biostatistics/kxi044

44. Ogden RT, Ojha A, Erlandsson K, Oquendo MA, Mann JJ, Parsey RV (2007) In vivo quantification of serotonin transporters using [¹¹C]DASB and positron emission tomography in humans: modeling considerations. J Cereb Blood Flow Metab 27(1):205–217. https://doi.org/10.1038/sj.jcbfm.9600329

45. Ogden RT, Zanderigo F, Choy S, Mann JJ, Parsey RV (2010) Simultaneous estimation of input functions: an empirical study. J Cereb Blood Flow Metab 30(4):816–826. https://doi.org/10.1038/jcbfm.2009.245

46. Collste K, Forsberg A, Varrone A, Amini N, Aeinehband S, Yakushev I, Halldin C, Farde L, Cervenka S (2016) Test-retest reproducibility of [¹¹C]PBR28 binding to TSPO in healthy control subjects. Eur J Nucl Med Mol Imaging 43(1):173–183. https://doi.org/10.1007/s00259-015-3149-8

47. Naganawa M, Zheng MQ, Henry S, Nabulsi N, Lin SF, Ropchan J, Labaree D, Najafzadeh S, Kapinos M, Tauscher J, Neumeister A, Carson RE, Huang Y (2015) Test-retest reproducibility of binding parameters in humans with ¹¹C-LY2795050, an antagonist PET radiotracer for the kappa opioid receptor. J Nucl Med 56(2):243–248. https://doi.org/10.2967/jnumed.114.147975

48. Bacher I, Houle S, Xu X, Zawertailo L, Soliman A, Wilson AA, Selby P, George TP, Sacher J, Miler L, Kish SJ, Rusjan P, Meyer JH (2011) Monoamine oxidase A binding in the prefrontal and anterior cingulate cortices during acute withdrawal from heavy cigarette smoking. Arch Gen Psych 68(8):817–826. https://doi.org/10.1001/archgenpsychiatry.2011.82

49. Soliman A, Bagby RM, Wilson AA, Miler L, Clark M, Rusjan P, Sacher J, Houle S, Meyer JH (2011) Relationship of monoamine oxidase A binding to adaptive and maladaptive personality traits. Psychol Med 41(05):1051–1060. https://doi.org/10.1017/S0033291710001601

50. Slifstein M, Laruelle M (2000) Effects of statistical noise on graphic analysis of PET neuroreceptor studies. J Nucl Med 41(12):2083–2088

51. Barth C, Villringer A, Sacher J (2015) Sex hormones affect neurotransmitters and shape the adult female brain during hormonal transition periods. Front Neurosci 9:37

52. Gundlah C, Lu NZ, Bethea CL (2002) Ovarian steroid regulation of monoamine oxidase-A and -B mRNAs in the macaque dorsal raphe and hypothalamic nuclei. Psychopharmacology 160(3):271–282. https://doi.org/10.1007/s00213-001-0959-0

53. Rekkas PV, Wilson AA, Lee VW et al (2014) Greater monoamine oxidase a binding in perimenopausal age as measured with carbon 11-labeled harmine positron emission tomography. JAMA Psych 71(8):873–879. https://doi.org/10.1001/jamapsychiatry.2014.250